PHYSICAL REVIEW B **104**, 035411 (2021)

Spectral features of magnetic domain walls on the surface of three-dimensional topological insulators

I. P. Rusinov[*]
Tomsk State University, Tomsk 634050, Russia

V. N. Men'shov
NRC Kurchatov Institute, Kurchatov Sqr. 1, 123182 Moscow, Russia
and Tomsk State University, Tomsk 634050, Russia

E. V. Chulkov
St. Petersburg State University, 199034 St. Petersburg, Russia;
Donostia International Physics Center (DIPC), 20018 San Sebastián/Donostia, Spain;
and Departamento de Polímeros y Materiales Avanzados: Física, Química y Tecnología,
Facultad de Ciencias Químicas, Universidad del País Vasco UPV/EHU, 20080 San Sebastián/Donostia, Basque Country, Spain

(Received 7 May 2021; accepted 23 June 2021; published 9 July 2021)

We present a theoretical investigation of electron states hosted by magnetic domain walls on the three-dimensional topological insulator surface. The consideration includes the domain walls with distinct vectorial and spatial textures. The study is carried out on the basis of the Hamiltonian for quasirelativistic fermions by using a continual approach and tight-binding calculations. We derive the spectral characteristics and spatial localization of the one-dimensional low-energy states appearing at the domain walls. The antiphase domain walls are shown to generate the topologically protected chiral states with linear dispersion, the group velocity and spin-polarization direction of which depend on an easy-axis orientation. In the case of an easy-plane anisotropy, we predict a realization of a dispersionless state flatband in the energy spectrum, that is spin polarized along the surface normal. Modification of the surface states in the multidomain case, which is approximated by a periodic set of domain walls, is described as well. We find that the magnetic domain walls with complex internal texture, such as Néel-like or Bloch-like walls, also host the topological states, although their spectrum and spin structure can be changed compared with the sharp wall case.

DOI: 10.1103/PhysRevB.104.035411

I. INTRODUCTION

The effect of quantized conductivity without an external magnetic field was revealed and studied in topological insulators (TIs) that are time-reversal invariant semiconductors with strong spin-orbit coupling [1–3]. However, namely, the breaking of time-reversal symmetry through the introduction of a magnetic order in TIs provides conducive ground for an emergence of fascinating phenomena such as quantum anomalous Hall effect (QAHE) [4–8], axion insulator state [8], and Majorana fermions [9], which would allow extending the potential of spintronic applications. At present, there are several viable approaches for creating a magnetic order in TIs on the basis of tetradymitelike semiconductors [10]. Accordingly, five alternative platforms suitable for realization of phenomena associated with quantized transverse conductivity can be outlined as follows. (1) QAHE was first detected in thin films composed of a few quintuple layers (QLs) of TIs $\mathrm{Cr}_x(\mathrm{Bi,Sb})_{2-x}\mathrm{Te}_3$ [11] and $\mathrm{V}_x(\mathrm{Bi,Sb})_{2-x}\mathrm{Te}_3$ [12], where randomly dissolved moments of transition metal atoms form ferromagnetic (FM) long-range order. (2) By using magnetic modulation doping, when the rich-Cr/V-doped thin layers are inserted near both the surfaces of $(\mathrm{Bi,Sb})_2\mathrm{Te}_3$ films, experimentalists have succeeded in observing QAHE [13–15] and axion insulator state [15–17]. (3) The magnetic-proximity-effect-induced QAHE has been implemented in the $(\mathrm{Zn,Cr})\mathrm{Te}/(\mathrm{Bi,Sb})_2\mathrm{Te}_3/(\mathrm{Zn,Cr})\mathrm{Te}$ heterostructure due to a fine-tuning of the composition of FM insulator interfaced with TI [18]. (4) The giant exchange gap at the Dirac point of the surface state could be achieved due to a magnetic extension effect, when a thin layer of FM insulator is deposited on the surface of a nonmagnetic TI, which are both structurally and compositionally compatible with each other [19,20]. Perhaps this effect is responsible for anomalous Hall regime at temperatures of several Kelvin observed in the magnetic topological bulk crystals in which Mn ions self-organize into a periodic $\mathrm{MnBi}_2\mathrm{Te}_4/\mathrm{Bi}_2\mathrm{Te}_3$ superlattice [21]. (5) Recently, the existence of quantized Hall conductivity, accompanied by zero longitudinal resistance, was experimentally demonstrated in the thin flakes of an intrinsic antiferromagnetic (AFM) TI $\mathrm{MnBi}_2\mathrm{Te}_4$ with odd numbers of septuple layers (SLs), concretely five SLs, under zero extrinsic magnetic field [22]. This is a typical behavior of QAHE, theoretically predicted for

---

[*] Corresponding author: rusinovip@gmail.com

intrinsic AFM TI in Ref. [23]. In turn, the flakes of $\mathrm{MnBi_2Te_4}$ with even number of SLs, namely, six SLs, have exhibited axion insulator state at zero magnetic field [24].

Despite rapid progress in this field, the exploration of magnetic TIs with in-plane easy axis [25–27] or with magnetic moment canted towards the surface [28,29] remains scarce. The recent study [30] has predicted the in-plane sublattice magnetization in the vanadium-based family of AFM TIs $\mathrm{V(Bi, Sb)_2(Se, Te)_4}$, which could significantly broaden the base for the search of exotic fermion states at the TI surface.

It should be stressed that, in the magnetic TI samples prepared for spin-dependent transport measurements, the physical boundaries such as surfaces, interfaces, and side faces play a particular role [8,10]. Conceptually, given that the surface/interface states are fully gapped at the Dirac point due to the spontaneous magnetization normal to the surface, the topologically protected edge chiral channels running along the side faces are responsible for the quantized Hall conductivity [4–8,10]. In reality, the magnetization distribution at the surface can be highly distinct from the bulk magnetic order. It is thought that this distinction can be caused by various factors. One of them is thermal magnetization fluctuations which, as a rule, are enhanced in the surface region of a magnetic systems [31]. At the same time, the magnetic fluctuations are frozen by static symmetry-reducing imperfections [32]. The structural defects and compositional disorder inevitably occur during the exfoliation or the epitaxial growth of the TI samples [33–35]. For instance, the surface of an exfoliated $\mathrm{MnBi_2Te_4}$ flake can even be subjected to strong chemical reconstruction, so that the topmost SL becomes rather as a Mn-doped $\mathrm{Bi_2Te_3}$ and a $\mathrm{Mn}_x\mathrm{Bi}_y\mathrm{Te}$ double layer with a clear van der Waals gap in between [36]. These and other symmetry-reducing imperfections can dominate locally the exchange and dipolar interactions between moments as well as magnetic anisotropy at the surface. In turn, an interplay between the exchange coupling and anisotropy drives nucleation and energetic stability of the magnetic landscape at the terminating surface including complex space-varying textures of magnetization. It is also important to emphasize that, in tetradymite TI materials, the topologically protected surface states are mostly localized inside a few terminating QLs/SLs, i.e., roughly speaking, inside the same region where the magnetic order is sensitive to the perturbations and therefore can be remarkably modified compared with the bulk magnetic order.

The existence of magnetic domain walls (DWs) on the surface of magnetic TIs and the one-dimensional (1D) electron states associated with them is experimentally confirmed [35,37,38]. Using magnetic force microscopy, Sass and co-authors presented microscopic evidence of the DWs on the as-grown (0001) surface of $\mathrm{MnBi_2Te_4}$, which is consistent with opposite surface magnetizations of antiphase domains or terraces separated by SL steps [35]. The emergence of multidomain states at topological phase transitions under external field sweep was found in various magnetic systems based on TIs [15,17,37–41]. The inconsistency of spectroscopy [angle-resolved photoemission spectroscopy (ARPES)] results [42–45] with the earlier ones [29,46–48] indicates the possibility of a spatially inhomogeneous structure of the surface magnetization in $\mathrm{MnBi_2Te_4}$. In addition, the magnetic DWs on the AFM TI surface could also be induced intentionally using a magnetic force microscope tip [49] or by spatially modulated external magnetic field due to Meissner repulsion from a bulk superconductor, as has been realized in Cr-doped TI $\mathrm{(Bi, Sb)_2Te_3}$ [50]. On the theoretical side, the issue on particular quasiparticle states on the magnetic DWs of TIs was raised previously in Refs. [30,51–56].

In this work, we study how the magnetic inhomogeneities such as DWs can modify a picture of the topological surface states. The DW spatial textures are modeled as static one-dimensional boundaries between magnetic domains of different orientations on the TI surface. We discuss the properties of the DW-induced fermion states in the context of the real space localization and the spin-resolved spectral function. We demonstrate that such DWs host topologically protected chiral fermion states, the energy spectrum of which can evolve from a linear dispersion to a flatband depending on the easy-axis orientation. The results are obtained by means of two complementary methods: one based on the effective low-energy Dirac equation description and the other based on a numerical tight-binding approach.

The rest of the paper is organized as follows. In Sec. II we present the microscopic model of DWs on the magnetic TI surface and outline methodological details of the description of the electron states bound to DWs. In Sec. III, we successively investigate the characteristics of the low-energy surface states generated by a single magnetic antiphase DW under different directions of easy axis, a pair of the antiphase DWs, and the multidomain periodic configurations of magnetization. Here we also study how the noncollinear and noncoplanar textures of the magnetization modify the spectral properties of the surface states. Finally, in Sec. IV, we summarize the obtained results and discuss possible manifestations of DWs in spectroscopy and transport properties of TIs.

II. MODEL AND METHODS

The essential low-energy physics on the 3D TI surface can be described by massless two-component fermions with the spin-momentum locking [1–3]. In the presence of the exchange field at the surface, the motion of the fermions can be modeled with the effective two-dimensional (2D) Hamiltonian

$$H(\mathbf{k}) = -v[\mathbf{k} \times \boldsymbol{\sigma}]_z + J(\mathbf{M} \cdot \boldsymbol{\sigma}). \tag{1}$$

Here, the first term is the lowest-order expansion of the Dirac quasiparticle energy in the small in-plane momentum $\mathbf{k} = (k_x, k_y)$ around the $\overline{\Gamma}$ point in the surface Brillouin zone (BZ), v is the Fermi velocity (one assumes $\hbar = 1$), and $\boldsymbol{\sigma}$ is the trio of Pauli matrices σ_i $(i = x, y, z)$ for the spin degree of freedom. In the tetradymite TI systems, both in the case of randomly distributed *3d* transition metal dopants and in the case of regularly aligned layers of magnetic ions, the exchange coupling is mediated by p orbitals of the TI host. It can lead to the appearance of a magnetic ordering and hence a surface magnetization $\mathbf{M}(x, y)$. The latter causes a spin polarization of the Dirac fermions owing to an effective interaction J. We present the corresponding exchange energy by the second term in Eq. (1) that allows us to capture the DW fingerprints in the spectral properties of the surface electrons in any of the five platforms for magnetic ordering in the TIs listed above.

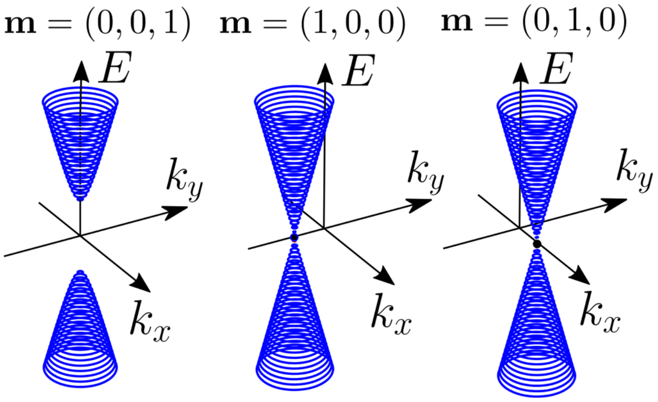

FIG. 1. Energy dispersion in the momentum space (k_x, k_y) for topological surface state subjected to the uniform surface magnetization oriented along the z axis (left panel), the x axis (central panel), and the y axis (right panel).

It should be noted that the interaction strength J depends profoundly on the strategy of the formation magnetic order in the system. We also suppose that the interaction J is the same in the in-plane and out-of-plane direction (for certainty $J > 0$) and ignore the particle-hole asymmetry in the surface bands. We suggest that the surface states modeled with Eq. (1) reside in the projected bulk band gap. It should be noted, we do not include a possible hexagonal warping term [57,58], which could be avoided at small momentum near the BZ center.

If the surface magnetization is uniform, the energy spectrum of the Hamiltonian (1) is given by the relation $E^2 = (\nu k_x - JM_y)^2 + (\nu k_y + JM_x)^2 + J^2M_z^2$. Thus, when the vector $\mathbf{M}$ is oriented in the surface plane, the 2D electron states show a gapless cone spectrum with the Dirac point shifted from the BZ origin in the direction perpendicular to $\mathbf{M}$. In the case of out-of-plane easy axis, the surface states are gapped. The corresponding 2D spectral relations for the three orientations of the uniform surface magnetization are illustrated in Fig. 1. However, for topological surface states, an interplay of the band topology and magnetic ordering is not reduced to these spectral features. Indeed, the topological indices of the surface states of a magnetic TI might be closely linked with the sign of either the exchange energy gap or the exchange shift of the Dirac cone in the 2D BZ, depending on the magnetic easy-axis direction. In other words, the fermions moving on the magnetically inhomogeneous surface can acquire the spatially varying topological indices. Thus, the DW, across which the surface magnetization changes its sign, is also a border separating domains with different topological indices. Thereby, such a border is expected to host a peculiar topologically protected 1D state.

As emphasized above, despite the presence of magnetic order in the TI bulk, the terminating surface can display rather considerable local variations of the magnetization $\mathbf{M}(x, y)$, including DWs with various textures. The magnetic DWs of certain types can bind the Dirac fermions. In order to elucidate this issue, we address a particular class of magnetic configurations in which the $\mathbf{M}$, magnitude, is fixed, $|\mathbf{M}(x, y)| = M_0$, while the vector $\mathbf{M}(x, y)/M_0 = \mathbf{m}(x, y)$ is a function of the position at the surface plane. Furthermore, we restrict our study to a 1D model in the sense that the magnetization undergoes large-scale modulation in only one spatial direction, for definiteness $\mathbf{m}(x, y) \to \mathbf{m}(x)$, while retaining lattice periodicity in the orthogonal direction and, consequently, conserving momentum k_y. We consider several representative orientation configurations of the surface magnetization. We do not analyze here the energy of these configurations, but make use of them as a playground for the exploration of substantive characteristics of the topological surface states. At first, we will address isolated antiphase DWs of zero width such as $\mathbf{m}(x) = \mathbf{m}_0\,\mathrm{sgn}(x)$, which may differ in the $\mathbf{m}_0$ direction with respect to the crystallographic axes of the system. If the distance between the neighboring DWs is not too large, the DW-induced bound states overlap and hybridize. This aspect is explored by using configurations of a pair of DWs and a 1D periodic domain lattice. We also consider noncollinear magnetic DWs at the TI surface and study the bound states appearing at the isolated 180° Néel-type and Bloch-type DWs, which profiles are simulated by piecewise unit vectors $\mathbf{m}$.

Our k-linear model approach, Eq. (1), has the advantage that it allows us to readily explain the main trends in modification of the topological surface states caused by perturbations of magnetization that are not easily accounted for within *ab initio* simulations. We employ both the continuum model analysis and the tight-binding calculations. The former is used to find explicit low-energy solutions for the Dirac-like equation. The latter are based on a lattice regularization of the $\mathbf{k}\cdot\mathbf{p}$ Hamiltonian (1) via the substitution $k_{x,y} \to (1/a)\sin(k_{x,y}a)$ where a is a 2D square lattice constant. The tight-binding simulation is featured by the dimensionless parameter JM_0a/ν. To avoid an appearance of false Dirac points at the boundary of BZ, known as the double-fermion problem [59], we include the Wilson mass term $\frac{2w\sigma_z}{a^2}[2 - \cos(k_xa) - \cos(k_ya)]$, which does not significantly affect the surface state behavior at small momenta. The tight-binding calculations are performed using a recursive technique for the Green's functions [60,61]. Having obtained the retarded Green's function $[G^R(E, k_y)]$ for a given magnetization distribution, we can analyze further the corresponding momentum-resolved one-particle spectral function $\rho(E, k_y) = (-1/\pi)\mathrm{Im}\,\mathrm{Tr}\,G^R(E, k_y)$ and that for each spin polarization $S_i(E, k_y) = (-1/\pi)\mathrm{Im}\,\mathrm{Tr}\,\sigma_i G^R(E, k_y)$. Furthermore, we can obtain the total density of states (DOS) $\rho(E) = (2\pi/a)\int_{-\pi/a}^{\pi/a} dk_y \rho(E, k_y)$, and the net spin polarization $S_i(E) = (2\pi/a)\int_{-\pi/a}^{\pi/a} dk_y S_i(E, k_y)$ as a function of the state energy, E. The spatial distribution of the surface electron state is evaluated by the local density of states $\rho(E, x, k_y) = (-1/\pi)\mathrm{Im}\,[E + i\epsilon - H(x, k_y)]^{-1}$ at energy E, where $i\epsilon$ is a small broadening width. The results of the tight-binding numerical simulations are presented in Figs. 2–9.

III. THE MAIN RESULTS

A. Single antiphase domain wall

We begin by considering the electron state bound to a single collinear DW, when two of its sides differ in sign of the magnetization. For definiteness, DW is assumed to extend along the y direction being centered at $x = 0$. The spatial configuration of such an antiphase DW is merely given by a step function profile, $\mathbf{m}(x, y) = \mathbf{m}(x) = \mathbf{m}_0\,\mathrm{sgn}(x)$, i.e., the DW magnetization changes sharply its direction

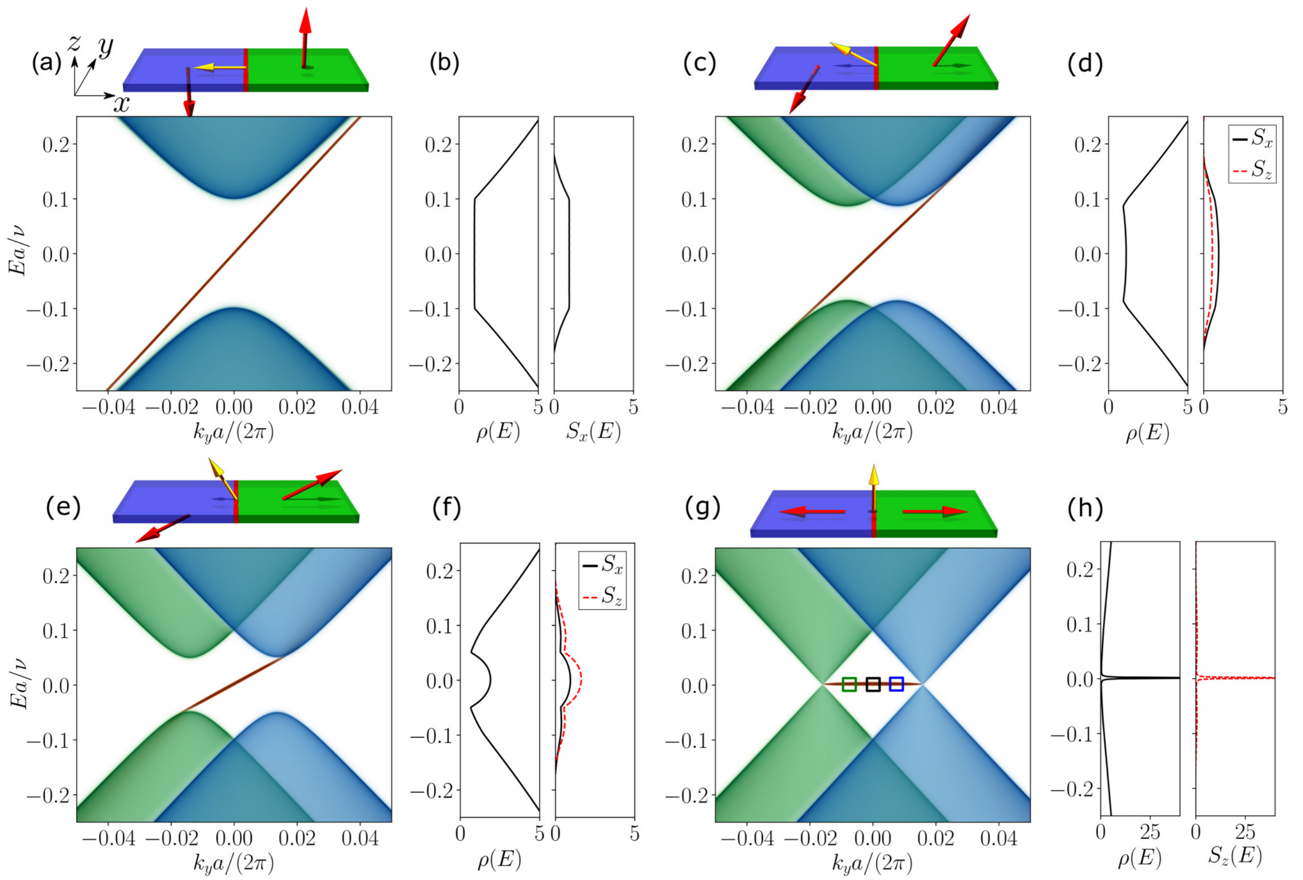

FIG. 2. Bound electron states induced by a single sharp antiphase DW on the magnetic TI surface for increasing angle θ. Panels (a),(b), (c),(d), (e),(f), and (g),(h) correspond to $\theta = 0$, $\pi/6$, $\pi/3$, and $\pi/2$, respectively. Projected topological surface bands associated with left and right magnetic domains are in blue and green, respectively. In panel (a) these bands coincide. Dependence $E(k_y)$ for the DW-induced bound state obtained in terms of spectral function is in red. The total DOS, $\rho(E)$, and the spin polarization, $S_i(E)$, are shown as well. The top of panels (a), (c), (e), and (g) contains the schematic image of magnetic texture of the antiphase DW indicated by arrows.

to just the opposite one under crossing over the boundary $(x = 0, y)$, while the magnetization within the domain stays uniform. We describe the unit vector $\mathbf{m}_0 = [\cos(\phi)\sin(\theta), \sin(\phi)\sin(\theta), \cos(\theta)]$ with spherical coordinates, where the polar angle θ and azimuthal angle ϕ set the magnetization orientation with respect to the z axis and in the surface plane (x, y), respectively. The vector $\mathbf{m}_0$ is typically aligned with the magnetic easy axis. The infinitely thin DW approximation is justified, provided that the DW width is significantly shorter than the localization scale of the electron state.

The system homogeneity along the y direction implies that the Bloch excitation with wave vector k_y propagates along the DW. Therefore, upon replacement $k_x \to -i\partial_x$, the problem is reduced to the 1D real-space Dirac equation $H(x, k_y)\Theta(x, k_y) = E(k_y)\Theta(x, k_y)$ for the bispinor envelope function $\Theta(x, k_y) = [\varphi(x, k_y), \chi(x, k_y)]^{\mathrm{T}}$, which must decay into the domain regions, i.e., $\Theta(|x| \to \infty, k_y) = 0$. On the other hand, the function $\Theta(x, k_y)$ satisfies the boundary conditions that ensure its continuity at $x = 0$ and the derivative jump which reads

$$\begin{aligned} i\sigma_y[\partial_x\Theta(x, k_y)|_{0^+} - \partial_x\Theta(x, k_y)|_{0^-}] \\ = 2k_0(\mathbf{m}_0\cdot\boldsymbol{\sigma})\Theta(0, k_y), \end{aligned} \tag{2}$$

where $k_0 = JM_0/\nu$ is the characteristic momentum.

As a prime example of the eigenproblem we address the case when the magnetization is tilted in the (x, z) plane by angle θ and the m_y component is absent, i.e., $\sin(\phi) = 0$. The "tail-to-tail" DW, the two sides of which differ by angle π (for definiteness $0 \leqslant \theta \leqslant \pi/2$), harbors the bound state featured by the envelope function

$$\Theta(x, k_y) = \Theta_0\begin{pmatrix}\alpha\\1\end{pmatrix}\sum_{\pm} h(\pm x)\exp(\mp p_\pm x) \tag{3}$$

and the energy dispersion

$$E(k_y) = \nu k_y\cos(\theta). \tag{4}$$

Here $h(x)$ is the Heaviside function, the momenta $p_\pm = k_0 \pm k_y\sin(\theta)$ determine the localization length of the bound state, and Θ_0 is a normalization constant, $\alpha = \tan[(\pi/2 - \theta)/2]$. The spectral branch (4) exists within the momentum interval $|k_y\sin(\theta)| < k_0$, where $p_\pm > 0$; in other words, the 1D linearly dispersive mode (4) meets the 2D Dirac cones when $|k_y\sin(\theta)| = k_0$.

Thus, we find that at the TI surface there is only one chiral bound state per single magnetic DW, propagating along the DW with group velocity $\nu_* = \nu\cos(\theta)$. The properties of the

DW-induced state (3)–(4) alter as one changes the tilt angle θ. When the domain magnetization is parallel to the surface normal, the emergent state is massless linearly dispersing and completely spin polarized along the x-axis fermion with energy $E = \nu k_y$ and spinor construction $\alpha = 1$. On the contrary, when the vector $\mathbf{m}$ is parallel to the x axis, a heavy fermion with $E = 0$ and spin polarization along the z axis ($\alpha = 0$) appears. In any case, i.e., at arbitrary angle θ, one can see that the spin polarization of the bound state (3)–(4) is exactly perpendicular to both the DW propagation direction and the domain magnetization, $(\mathbf{m}_0 \cdot \langle\boldsymbol{\sigma}\rangle) = 0$. In this sense, besides spin-momentum coupling, the fermion state possesses a peculiar sort of chirality when the fermion spin localized at the DW is tightly locked to the surface magnetization. The DOS for the solution (3)–(4) is given by

$$\rho(E) = \frac{a}{2\pi\nu\cos(\theta)} h[\nu k_0 \cot(\theta) - |E|]. \tag{5}$$

The DOS (5) is transformed from the constant value $\rho(E) = a/(2\pi\nu)$ for $\theta = 0$ to the utterly narrow peak $\rho(E) = (ak_0/\pi)\delta(E)$ for $\theta = \pi/2$, where $\delta(E)$ is the delta function.

We have also numerically verified the existence and peculiarities of the DW-induced bound states using the lattice approximation. In the tight-binding calculations, the model dimensionless parameter is chosen as $JM_0 a/\nu = 0.1$ only for convenience, in order to facilitate the visualization of the results. One can easily verify that the same qualitative results would be observed for any value of this parameter. In Fig. 2, we plot representative pictures of the spectral dependencies, $E(k_y)$, the total DOS, $\rho(E)$, and the spin polarization, $S_i(E)$, for four selected values of the angle θ; in addition, the corresponding DW configurations are schematically depicted. What we are most interested in is the low-lying states in the middle of the projected 1D BZ $|k_y| < \pi/a$ with the momenta that are small compared to the momentum of the order of the reciprocal lattice length. First, the energy spectrum of these states comprises pronounced projections of the two Dirac cones, originated from the corresponding magnetic domains, separated by momentum $2k_0\sin(\theta)$ and gapped by energy $2JM_0\cos(\theta)$. Second, and most important, there is a 1D massless linearly dispersing in-gap chiral fermion branch [at $\cos(\theta) \neq 0$] associated with the DW-induced bound state. The properties of the emergent DW states controlled by the polar angle are drastically different in the cases when the easy axis is normal to the surface or lies in its plane. As seen in Figs. 2(a) and 2(b), at $\cos(\theta) = 1$, the fully spin polarized along the x-axis dispersionless mode with constant DOS spans the exchange gap of the size $2JM_0$ in the Dirac cone. Away from the angle $\theta = 0$, the state gradually changes its character: the group velocity, $\nu_* = \nu\cos(\theta)$, of the bound state reduces linearly with the m_z component, the spin polarization deviates from the x axis in the (x, z) plane, and DOS as a function of energy concentrates around $E = 0$. Particular cases are demonstrated in Fig. 2 for $\theta = \pi/6$ [panels (c) and (d)] and for $\theta = \pi/3$ [panels (e) and (f)]. Eventually, at $\cos(\theta) = 0$, one observes in Fig. 2(g) a perfectly flat band with energy $E = 0$ that bridges the two Dirac cones with nodes at momenta $\pm k_0$. The corresponding heavy fermion state, fully spin polarized along the z axis, manifests in a dramatic enhancement of DOS [Fig. 2(h)]. In Fig. 3 we depict the local density profile of the flatband state for three momenta k_y.

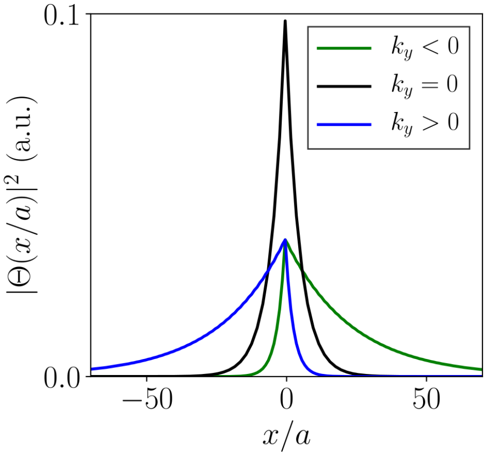

FIG. 3. Spatial profiles of the probability density of the planar DW bound state for distinct momenta k_y indicated with small color squares on the dispersion curves in Fig. 2(g).

Thus, combining analytic model and tight-binding numerical simulations in the long-wavelength limit we consistently demonstrate that the antiphase DW at any polar orientation θ supports the in-gap chiral degenerate bound state. The chirality consists in locking of three vectors that are mutually orthogonal to each other, that is to say, they constitute the orthogonal trio: the domain polarization $\mathbf{m}_0$ (oriented as a rule along a favoring axis of a magnetocrystalline anisotropy in the surface plane), the state spin polarization $\langle\boldsymbol{\sigma}\rangle$, and the propagation direction, i.e., the wave vector $\mathbf{y}k_y$. The inversion of the DW magnetization $\mathbf{m}(x)$, such as tail-to-tail↔“head-to-head,” entails the alteration of the vectors $\langle\boldsymbol{\sigma}\rangle$ and $\mathbf{y}k_y$ to just the opposite ones. In other words, the fermions moving on the tail-to-tail and head-to-head DWs have the opposite chiralities.

The spectral and spin features of the DW-induced state are highly sensitive to the orientation of $\mathbf{m}_0$ with respect to the surface normal. Notably also, the existence of the eigen localized solution (3)–(4) is guaranteed by the antiphase DW texture, which allows us to consider such a magnetic defect as a topological boundary and, consequently, the emergent in-gap quasiparticle state as a topologically protected one. When the magnetization points perpendicular to the TI surface, an exchange-interaction-induced magnetization opens up the gap of the size $2JM_0$. At the boundary between up and down out-of-plane magnetic domains, according to the known arguments [62,63], a chiral linearly dispersive state appears [Fig. 2(a)] because of the inversion of the gap from $+2JM_0$ to $-2JM_0$. To provide compelling evidence that the DW-induced state (3)–(4) has a topological origin at any polar angle, we use the reasoning similar to that given in Refs. [30,64]. In the general case, which is addressed here, the role of the “effective gap” could be played by the momentum-dependent energy parameter $\Delta(x, k_y) = 2\nu[p_+h(x) - p_-h(-x)] = 2[JM_0\,\mathrm{sgn}(x) + \nu k_y\sin(\theta)]$. Provided that k_y is restricted to the realm of the existence of the bound state (3)–(4) in the 1D BZ, $|k_y\sin(\theta)| < k_0$, the parameter $\Delta(x, k_y)$ changes its sign just at the magnetic DW.

On the contrary, if $|k_y \sin(\theta)| > k_0$, the parameter $\Delta(x, k_y)$ has the same sign on both sides of the DW. Thus, the 1D gapless surface bound state (3)–(4) appears due to the "gap" $\Delta(x, k_y)$ closing at the DW, which is guaranteed by the texture of the antiphase DW at any polar orientation θ. In the partial case of the easy plane, $\theta = \pi/2$, the linearly dispersing branch of the surface spectrum, Figs. 2(a), 2(c) and 2(e), transforms into the flatband branch with energy $E = 0$ connecting the Dirac points at $k_y = \pm k_0$, Fig. 2(g). It should be acknowledged that the existence of a 2D dispersionless state, so-called "heavy fermion," was predicted by Volkov and Pankratov in the case of a supersymmetric DW in a ferroelectric semiconductor A^4B^6 [65].

When the surface magnetization remains in the (y, z) plane, the antiphase DW featured by the vector $\mathbf{m}_0 = [0, \sin(\theta), \cos(\theta)]$ hosts massless linearly dispersing chiral fermions for any angle $0 \leqslant \theta \leqslant \pi/2$. According to the boundary conditions of Eq. (2), it is described by the envelope function $\Theta(x, k_y) \sim \exp(-k_0 e^{i\theta}|x|)$ and spectrum $E(k_y) = \nu k_y$ and is fully spin polarized along the x axis. In the case in which the magnetization is oriented along the DW, i.e., $\theta = \pi/2$ and $\varphi = \pi/2$, the bound state disappears.

B. The flatband state for a single domain wall with in-plane magnetization

Now we turn to consideration of the magnetic TI surface where domains are oriented in the basic plane due to preferable easy-plane anisotropy. In order to understand what happens with the surface state, we set the single azimuthal DW that separates two regions with differing magnetization orientations specified by angles ϕ_+ and ϕ_-. The magnetization spatial profile reads $\mathbf{m}(x) = [\cos(\phi_+), \sin(\phi_+), 0]h(x) + [\cos(\phi_-), \sin(\phi_-), 0]h(-x)$. We find readily the DW-induced state pinned to energy $E = 0$ and express its envelope function as

$$\begin{aligned}\Theta(x) &= \begin{pmatrix}\varphi_0\\ 0\end{pmatrix}\sum_{\pm} h(\pm x)\exp(q_\pm x),\\ &\quad -k_0\cos(\phi_-) < k_y < -k_0\cos(\phi_+);\\ \Theta(x) &= \begin{pmatrix}0\\ \chi_0\end{pmatrix}\sum_{\pm} h(\pm x)\exp(-q^*_\pm x),\\ &\quad -k_0\cos(\phi_+) < k_y < -k_0\cos(\phi_-),\end{aligned} \tag{6}$$

where the momenta $q_\pm = k_y + k_0\exp(i\phi_\pm)$ determine the localization length of the bound state, and φ_0 and χ_0 are normalization constants. From here we conclude that the azimuthal DW generates the dispersionless bound state with perfect spin polarization aligned perpendicular to the surface plane unless only the M_x components coincide. The realm of the flatband connecting the projections of the two Dirac cones in the 1D BZ is determined by angles ϕ_+ and ϕ_-. The condition $\phi_+ = -\phi_-$ or $\phi_+, \phi_- = \pm\pi/2$ means disappearing of the bound state. On the contrary, in the case of the antiphase DW, when either $\phi_+ = 0, \phi_- = \pi$ or $\phi_+ = \pi, \phi_- = 0$, the state occupies the widest possible realm in the momentum space, $|k_y| < k_0$, Fig. 2(g). The DOS for the flatband state of Eq. (6) is given by $\rho(E) = [ak_0/(2\pi)]|\cos(\phi_+) - \cos(\phi_-)|\delta(E)$. Our consideration demonstrates that the 1D flatband state is robust even when the orientations of the magnetic domains are rotated with respect to each other in the basic plane.

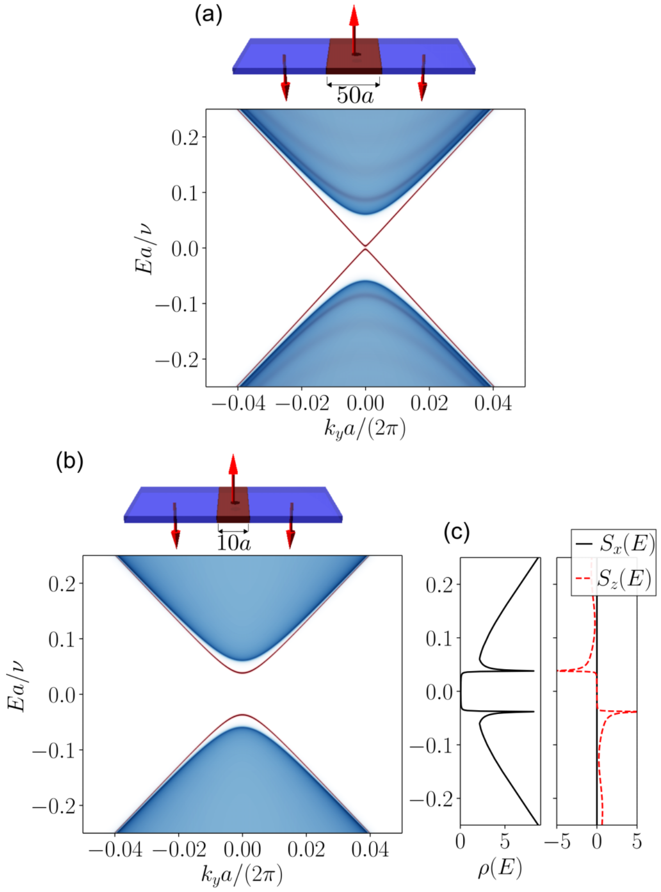

FIG. 4. Bound electron states induced by a pair of single sharp antiphase DWs on the magnetic TI surface for out-of-plane easy axis. Dependence $E(k_y)$ for the induced bound state obtained in terms of the spectral function is present in panels (a) and (b) in red for two different distances between DWs, $L = 50a$ and $L = 10a$. Total DOS, $\rho(E)$, and the spin polarization, $S_i(E)$, are shown in panel (c). The top of panels (a) and (b) contains the schematic image of out-of-plane antiphase magnetic texture, where the domain magnetizations are indicated by arrows.

C. Pair of antiphase domain walls

If the distance between two DWs is not too large, the DW-induced bound states can overlap and hybridize, effectively leading to a deformation of their spectra. To analyze this modification we describe the surface magnetization distribution as composed of three different regions divided by the sharp DWs fixed at $x = \pm L/2$. In the case of the out-of-plane anisotropy, the up-magnetized stripe domain of a finite width L is placed between the two half-infinite down-magnetized domains, which can be represented as $\mathbf{m}(x) = (0, 0, -1)h(|x| - L/2) + (0, 0, 1)h(L/2 - |x|)$. When the overlap of the tails of the states originating from the DWs is small, two 1D linear spectral branches appear within the exchange gap $2JM_0$, which are slightly gapped $\sim JM_0\exp(-k_0L)$ at $k_y = 0$ due to the states hybridization, Fig. 4(a). If the DWs are relatively

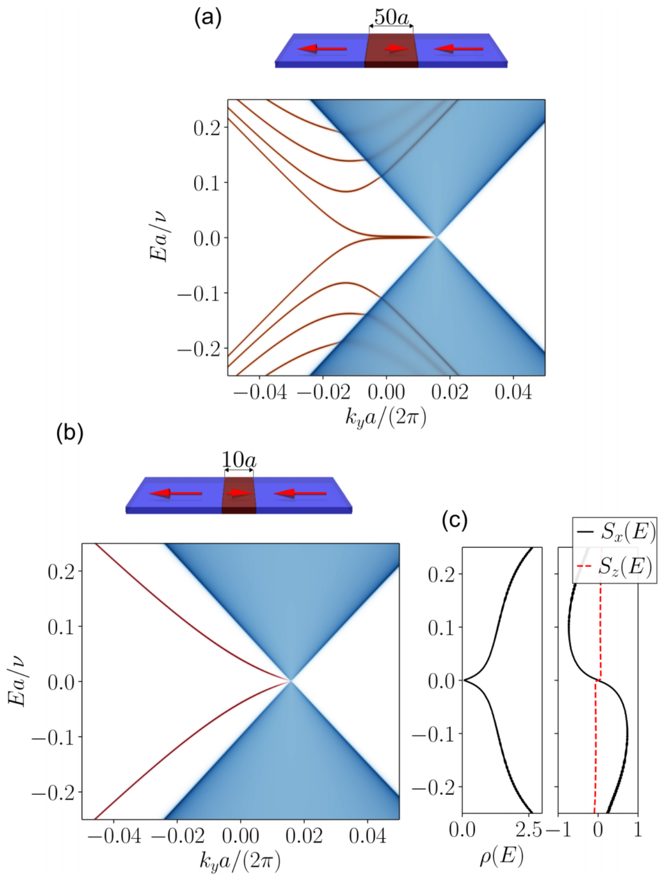

FIG. 5. The same as Fig. 4, but for the case of the in-plane easy axis.

close to each other, $Lk_0 \ll 1$, the large overlap leads to the formation of a pair of weakly localized states with paraboliclike bands [Fig. 4(b)], whose edges are near the exchange gap edges, $JM_0 - |E| \sim JM_0(k_0L)^2$ at $k_y = 0$. The DOS and spin polarization of these states are depicted in Fig. 4(c).

In the case of the in-plane anisotropy, the magnetization configuration includes the tail-to-tail and head-to-head DWs. For the sake of definiteness, we assume that the side domain regions magnetized along the x axis are separated by the intermediate region with the opposite magnetization direction, which is described by $\mathbf{m}(x) = (-1, 0, 0)h(|x| - L/2) + (1, 0, 0)h(L/2 - |x|)$. In the spectral picture of Fig. 5(a) one can see that, at large enough width L, one of the cones, associated with the middle domain, is weakly pronounced, while the heavy fermion spectral branch acquires weak dispersion given by $E(k_y) \approx \sqrt{2JM_0\nu(k_0 - k_y)}\exp[-(k_0 - k_y)L]$. When $Lk_0 \ll 1$, both this cone and the bound state disappear [Fig. 5(b)]. The respective DOS and spin polarization are depicted in Fig. 5(c). Our analysis shows that the DW-induced flatband state is highly sensitive to the DW-to-DW distance.

D. Periodical array of domain walls

In low-temperature phase, the surface of an as-grown magnetic material sample should host a set of domains with different magnetization directions [32,66,67]. Here the question arises as to how such a multidomain magnetic texture, in particular the domain length scale, affects the electronic and spin structure of the TI surface states. To figure that out, we address the 1D periodically modulated collinear textures of the surface magnetization which consist of alternating magnetization stripes aligned in the opposite directions: $\mathbf{m}(x) = \mathbf{m}_0\,\mathrm{sgn}[\sin(\pi x/L)]$, where $2L$ is the texture period. The domain stripes have finite width along the x axis and infinite length along the y axis and are separated from one another by sharp antiphase DWs. The net surface magnetization is supposed to be vanished. The domain polarization $\mathbf{m}_0$ is fixed to an easy axis. To be more specific, we study the modification of the topological surface states under the magnetic texture $\mathbf{m}(x)$ for two cases: the out-of-plane anisotropy, when $\mathbf{m}_0 = (0, 0, 1)$, and the in-plane anisotropy, when $\mathbf{m}_0 = (1, 0, 0)$.

The tight-binding calculations are performed using an enlarged unit cell, which is the stripe of width $2L = Na$ in the x direction, where N is the number of sites per the unit cell. The latter contains two antialigned domains. As we have already clarified, due to the local variation of exchange field, an isolated antiphase DW supports the bound state. As the magnetization forms a multidomain texture, the surface states stemming from the neighboring DWs hybridize. Hence, it is natural to expect that the surface Dirac-like spectrum rebuilds owing to the formation of the Bloch-like subbands $E_n(k_x, k_y)$ in the 2D BZ restricted to the realm $|k_y| < \pi/a$, $|k_x| < \pi/(2L)$.

In the case of the z easy axis, the 2D Dirac surface states are gapped out by the domain magnetizations pointing outwards and inwards from the sample surface, whereas the single DW produces the 1D in-gap state. As the DWs are arranged regularly, the low-energy spectrum can be expressed in the form $E_0^{\pm}(k_x, k_y) = \pm\sqrt{\nu^2k_y^2 + \xi^2(k_x) + \Delta^2}$. In the regime where the typical localization length k_0^{-1} is smaller than the inter-DW distance, the dispersion in k_x appears due to the weak overlap of the envelope function tails, $\xi(k_x) \sim \nu k_0 \exp(-k_0L)\sin(k_xL)$, the tiny hybridization gap 2Δ between the branches $E^+(k_x, k_y)$ and $E^-(k_x, k_y)$ is of the next order of magnitude in the overlap. The situation when the inter-DW distance is comparable to the typical localization length k_0^{-1} is illustrated by the spectral picture in Fig. 6 for $L = 30a$. Moreover, at the BZ boundary $|k_x| = \pi/(2L)$, the remarkable gap opens up in the spectral density of the propagating states about energy $|E| \approx 0.16\nu/a$ at $k_y \approx 0$. The x component of spin polarization $S_x(E, k_y)$ is depicted in Fig. 6 by means of color intensity of the spectral branches. This image tells about the spin-momentum locking of the surface states, excluding the narrow realm in the vicinity $k_y \approx 0$.

A more complicated situation arises in the case of the magnetization lying in the surface plane. When the adjacent DWs lie at quite some distance from one another, $L \gg k_0^{-1}$ [Fig. 7(a) for $L = 100a$], the flatness and spin polarization of the low-energy states near $E = 0$ changes very little as compared with the single-DW case. There occur the dispersion $\xi(k_x) \sim \nu k_0 \exp(-k_0L)\sin(k_xL)$ along k_x and the tiny gap 2Δ between the branches $E_0^+(k_x, |k_y| < k_0)$ and $E_0^-(k_x, |k_y| < k_0)$. As follows from Fig. 7(b), the spatial profile of the probability density of the low-energy state at $k_y \approx 0$ is significantly different from that at $|k_y| \approx k_0$. With regard to the delocalized states, as seen in Fig. 7(a) for the spectral density projected onto k_y, the continual cone spectrum is split into a

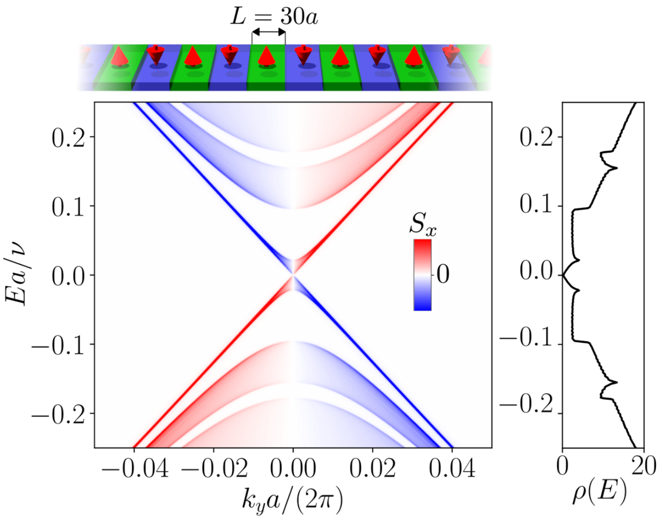

FIG. 6. Electron states induced by periodical array of sharp antiphase DWs on the magnetic TI surface with the out-of-plane easy axis. The spin-resolved spectral function is calculated for texture with the period $2L$, where $L = 30a$. The amplitude and sign of the spin polarization $S_x(E)$ of the energy states $E(k_y)$ are coded in a red-blue color scheme. The top of the panel contains the schematic image of the corresponding magnetic texture, where the domain magnetizations are indicated by arrows. Total DOS, $\rho(E)$, is shown as well.

set of subbands, $E_n(|k_y| = k_0) \approx \pi\nu n/(2L)$, $n = 1, 2, 3 \dots$. As the inter-DW distance is decreased to intermediate value $L \sim k_0^{-1}$, we find that the low-energy spectrum loses the flat behavior becoming parabolic along momentum k_y, which can be seen in Fig. 7(c) for $L = 30a$. Interestingly, while the bands at zero energy disappear, two new flatlike bands at the finite energy $|E| \approx \pm 0.13\nu/a$ emerge due to a rebuilding of the cone states in the exchange field of the periodic texture with $L = 30a$, Fig. 7(c). Correspondingly, two sharp peaks are present in the full DOS. One also notes that the component $S_x(E, k_y)$ reduces near $k_y \approx 0$, where the electron spin density is polarized normal to the surface. The real space behavior of some states with different eigenvalues is shown in Fig. 7(d).

Our analysis shows that the spectral characteristics of the low-energy states in the case of the z easy axis are generally stable in relation to varying inter-DW distance. On the contrary, in the case of the in-plane anisotropy, the dispersionless states bound to DW are highly sensitive to change of the distance between neighboring DWs. When $L \lesssim k_0^{-1}$, these states are interfering with each other shifting the flatband level from zero energy. As a result, the spectrum acquires the curvature and the gap. Moreover, the drastic redistribution of DOS of the 2D cone states takes place under the magnetization spatial modulation.

E. Noncollinear and noncoplanar domain walls

Above, we have considered the antiphase DW described by the collinear magnetization texture $\mathbf{m}(x) = \mathbf{m}_0 \operatorname{sgn}(x)$. Such a sharp profile is believed to be a reasonable approximation if the DW size is much smaller than the fermion localization length $\sim k_0^{-1}$; in this case, an internal structure of the DW is not important. Now we turn our attention to more complex DW textures displaying noncollinear and noncoplanar arrangement of the surface magnetization varying over finite scale. To explore the properties of the bound electron states induced by such textures, we address several typical examples of 1D 180° noncollinear and noncoplanar configurations, where the magnetization orientation varies only along the x axis, $\mathbf{m}(x) = [\mathbf{m}_x(x), \mathbf{m}_y(x), \mathbf{m}_z(x)]$, and the magnitude is fixed, $|\mathbf{m}(x)| = 1$. In order to avoid time-consuming calculations, we employ the approach where the spatial profile $\mathbf{m}(x)$ is composed of three differently oriented regions: $\mathbf{m}(x) = \mathbf{m}_\mathrm{s} h(|x| - l) \operatorname{sgn}(x) + \mathbf{m}_\mathrm{m} h(l - |x|)$, where $\mathbf{m}_\mathrm{s}$ and $\mathbf{m}_\mathrm{m}$ are independent of the coordinate, and the boundaries between the regions are perpendicular to the x axis. The magnetizations of the side regions, $\pm\mathbf{m}_\mathrm{s}$, are antiparallel to each other and orthogonal to that of the middle region, $\mathbf{m}_\mathrm{m}$, i.e., $(\mathbf{m}_\mathrm{s} \cdot \mathbf{m}_\mathrm{m}) = 0$. The approximation simulates a helical rotation or cycloidal one of the magnetization vector about the DW normal moving from one side to another for the Bloch-like texture or the Néel-like one, respectively. In the framework of our approach, the bound states created by these textures are described by solution of the eigenvalue problem $H(x, k_y)\Theta_n(x, k_y) = E_n(k_y)\Theta_n(x, k_y)$ with the Hamiltonian (1) under boundary conditions at $x = l$ and $x = -l$ presented in Eq. (2).

In the present approach, the coplanar vectors $\mathbf{m}_\mathrm{s} = (1, 0, 0)$ and $\mathbf{m}_\mathrm{m} = (0, 1, 0)$ set the Néel-like DW on the TI surface. The schematic of the magnetization profiles along the DW can be seen at the top of Fig. 8. A hallmark of this Néel-like DW is an existence of the dispersionless and strongly spin-polarized state with energy $E_0(k_y) = 0$ within the momentum interval $|k_y| < k_0$, at any width $2l$ of the middle region. When compared with the case of the sharp DW $\mathbf{m} = (1, 0, 0) \operatorname{sgn}(x)$ referred to in Eq. (3) at $\theta = \pi/2$, the presence of the middle region is reflected in the phase shift of the envelope function away from the DW core: $\Theta_0(x \to \pm\infty, k_y) \sim \exp(\mp|k_0 + k_y|x \pm ik_0 l)$. The spectral characteristics of the surface electrons are illustrated by the tight-binding simulations displayed in Fig. 8. They confirm clearly the existence of the flatband state and indicate a large sharp peak in both full DOS $\rho(E)$ and the spin polarization $S_z(E)$ near zero energy. It should be noted that in the case of a broad middle region, $l > k_0^{-1}$, the DW also supports the spin-degenerate gapped states with quasiparabolic bands $E_n(k_y) = E_n(-k_y)$ within the local gap in the 2D projected bands (Fig. 8), here $n = \pm 1, \pm 2, \dots \pm N$. The eigenstates have opposite energies with respect to the zero energy, $E_n(k_y) = -E_{-n}(k_y)$. With increasing the width, $2l$, a number of the gapped states, $2N$, grows. The bound states with $n \neq 0$ manifest in modification of DOS at the edges of the quasiparabolic bands. In the opposite case of the relatively sharp DW, when $l < k_0^{-1}$, the additional states with $n \neq 0$ do not occur. The specified above trends can be observed in Fig. 8 by comparing the spectral features for $2l = 50a$ and $2l = 20a$.

We performed a similar analysis of the bound states for the noncoplanar surface magnetic texture defined by the vectors $\mathbf{m}_\mathrm{s} = (0, 0, 1)$ and $\mathbf{m}_\mathrm{m} = (0, 1, 0)$, which is here referred to as the Bloch-like DW. We argue that, at any width of the middle region, the Bloch-like DW hosts the strongly spin-polarized

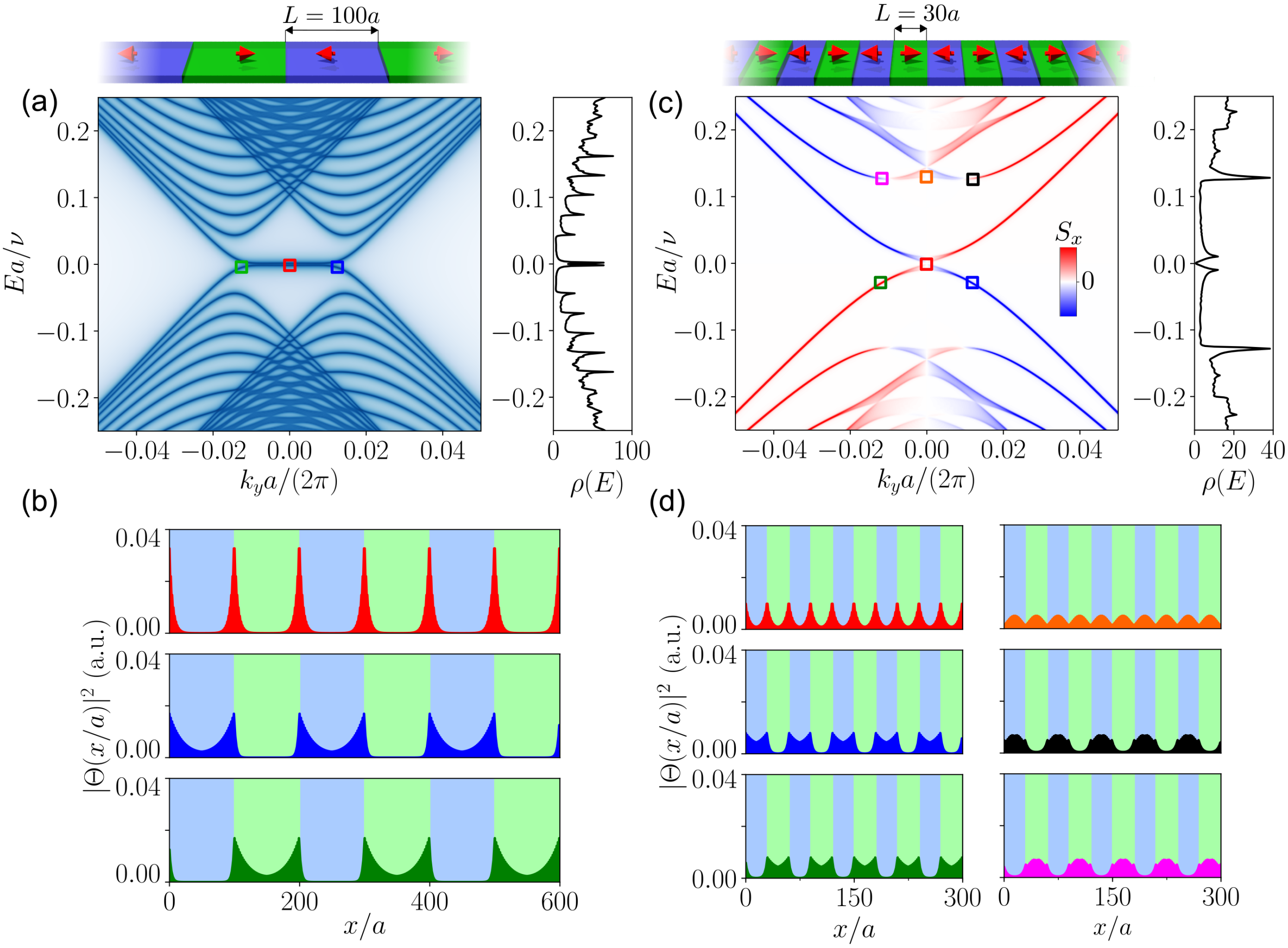

FIG. 7. Electron states induced by periodical array of sharp antiphase DWs on the magnetic TI surface for the in-plane easy axis. The calculated spin-resolved spectral function is shown for the texture with period $2L$, where $L = 100a$, in panel (a), and $L = 30a$, in panel (c). In the latter case, the amplitude and sign of the spin polarization $S_x(E, k_y)$ of the energy states $E(k_y)$ are coded in a red-blue color scheme. The top of panels (a) and (c) contains the schematic image of the corresponding magnetic texture, where the domain magnetizations are indicated by arrows. Total DOSs, $\rho(E)$, are shown as well. The panels (b) and (d) present spatial profiles of the probability density of the states with distinct momenta k_y indicated with small squares of the corresponding color on the dispersion curves in panels (a) and (c), respectively.

state with linear momentum-energy relationship $E_0(k_y) = \nu k_y$ spanning the exchange gap. The asymptotic behavior of the envelope function of the state away from the DW core, given by the relation $\Theta_0(x \to \pm\infty) \sim \exp[\mp k_0(x - il)]$ shows that the existence of the middle region results in a phase shift of the function. Furthermore, if the middle region is so wide that $l > k_0^{-1}$, the additional bound gapped states with quasiparabolic dispersion, $E_n(k_y) = E_n(-k_y)$ $(n = \pm 1, \pm 2, \dots \pm N)$, appear in the gap. These states are doubly degenerate in spin, and their spectrum is mirrored with respect to zero energy, $E_n(k_y) = -E_{-n}(k_y)$. With increasing $2l$, a number of the gapped states, $2N$, increases. In the case when $l < k_0^{-1}$, the additional states with $n \neq 0$ are absent.

Let us consider two polar Néel-like textures, where the surface magnetization is confined in the (x, z) plane. Figure 9 displays the spectral picture of the surface electron states for magnetic configuration given by $\mathbf{m}_\mathrm{s} = (1, 0, 0)$ and $\mathbf{m}_\mathrm{m} = (0, 0, 1)$. As seen in Fig. 9, in the case of the relatively wide middle region of $2l = 50a$, a pair of quasilinear bands appears within the local gap starting from the Dirac points at $k_y = \pm k_0$ and crossing at $k_y = 0$. This band crossing is accompanied by an opening of a tiny hybridization gap $\sim\exp(-2k_0 l)$, which divides the states with opposite spatial parity, $E_0(k_y)$ and $E_{-1}(k_y)$. As can be inferred by comparing the spectra at different values of the width $2l$ (see, e.g., the plots for $2l = 50a$ and $2l = 20a$ in Fig. 9), when the middle region is narrowed the gap $|E_0(0) - E_{-1}(0)|$ enlarges. At the same time, the low-energy dispersive state $E_0(k_y)$ sinks deeper into the local gap, and eventually in the small $2l$ limit, it takes the form of the perfect flatband close to zero energy connecting the two Dirac points, $E_0(k_y) \approx -2\nu k_0^2 l$ at $k_0 l \to 0$. Note also, that the state $E_0(k_y)$ is partially spin polarized at the finite width $2l$; however, it becomes a fully spin-polarized state if the DW middle region is completely shrunk. In turn, the state $E_{-1}(k_y)$ moves towards the band continuum edge and leaves the local gap below a certain value of the width $2l = k_0^{-1}$ $[E_{-1}(k_y) = -\nu k_0$ at $2k_0 l = 1]$.

One can also show that the two in-gap bound states are hosted by the Néel-like DW whose texture is defined by the vectors $\mathbf{m}_\mathrm{s} = (0, 0, 1)$ and $\mathbf{m}_\mathrm{m} = (1, 0, 0)$. Provided that the

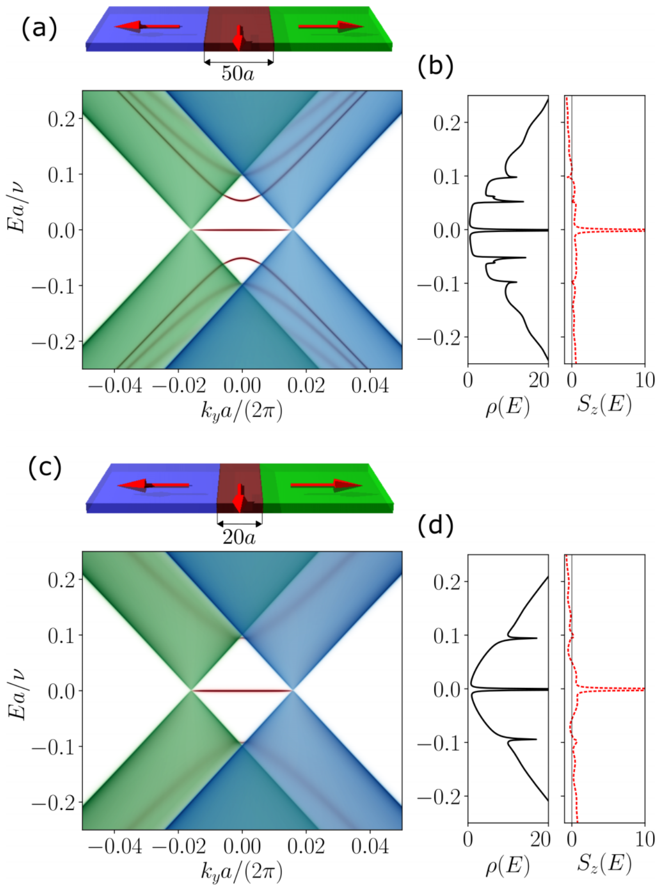

FIG. 8. Bound electron states induced by the Néel-like texture on the magnetic TI surface with the easy in-plane anisotropy. The spin-resolved spectral function is calculated for the texture with the middle region width $2l$, where $2l = 50a$ in panel (a) and $2l = 20a$ in panel (b). The top of the panels (a) and (c) contains the schematic image of the corresponding magnetic texture, where the right and left side regions are in green and blue, respectively, the middle region is in brown, and the arrows indicate the moments directions. The projected surface band structure associated with the left and right sides of the texture is in blue and green, respectively. The dependencies $E(k_y)$ for the DW-induced bound states are associated with red curves. The total DOS, $\rho(E)$, and the spin polarization, $S_z(E)$, are shown as well.

middle region is narrow enough, $k_0 l \ll 1$, one of these states leaves the exchange gap for the band continuum, while the other remains within the gap as the chiral fermion with the perfect linear dispersion $E_0(k_y) = \nu k_y$. It is evident that a single 90° DW, which contains the $(0, \pm 1, 0)$-oriented domain, does not support an in-gap bound state. However, noncollinear and noncoplanar 180° textures, in which the middle region magnetization $\mathbf{m}_\mathrm{m}$ is aligned along the y axis, can generate from one to several in-gap states. In any case, the 180° Néel- or Bloch-type DWs investigated certainly provide the existence of the topologically protected chiral state $E_0(k_y)$ inside the exchange gap.

IV. DISCUSSION AND SUMMARY

We have shown that the real-space magnetic textures, such as surface DWs, are capable of affecting substantially the momentum-space behavior of low-energy quasiparticles in TIs. Thus, any particular magnetization texture $\mathbf{M}(x, y)$ should provide its own spectral portrait for the surface electron states in the surface exchange gap. The averaged spectral function $A(E, \mathbf{k}) = -(1/\pi)\mathrm{Im\,Tr}\,\langle G^R[E, \mathbf{k}|\mathbf{M}(x, y)]\rangle$, in which the contributions of all the textures are collected according to their statistic weight, is thought to be observed in the spectroscopy measurements. Such an assumption may qualitatively explain controversial ARPES results for the surface spectra of intrinsic AFM TI $\mathrm{MnBi_2Te_4}$ with out-of-plane easy axis obtained by various experimental groups [34,42–44,46]. In the seminal work [46] a clear exchange gap of about 70 meV at the $\overline{\Gamma}$ point separating the upper and lower parts of the surface cone was revealed, which is close to the theoretically predicted value 88 meV. However, Shikin *et al.* [34] have found in the ARPES spectra both large (60–70 meV) and reduced (<20 meV) surface gaps at the Dirac point. Some other ARPES measurements [42–44] have detected the gapless Dirac states at the surface of $\mathrm{MnBi_2Te_4}$ below the Néel temperature instead of the expected exchange gapping of the states. Within the developed theory, we speculate that in the experimental findings cited here above the ARPES surface spectra may contain a superposition of the DW-induced spectral features like the ones presented in Figs. 2, 4, and 6 averaged spatially over multiple DWs caught out in the light

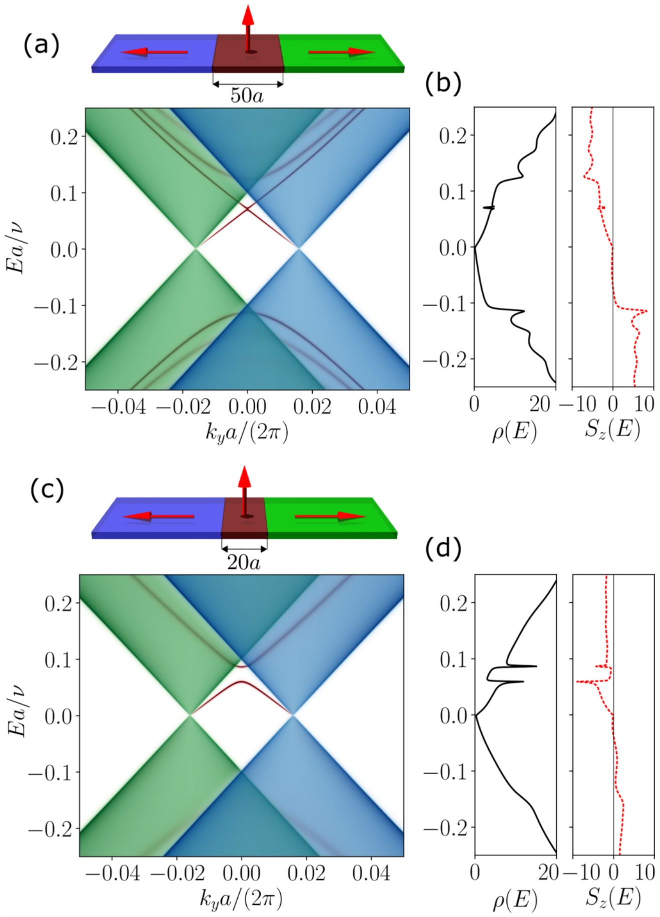

FIG. 9. The same as Fig. 8, but for the case of polar Néel-like texture.

spot of a micron scale. If the concentration of the DWs is relatively low, they can hardly ensure a visible spectral signal inside the large exchange gap, which is associated with almost homogeneous out-of-plane magnetization of the broad domains. With the increasing concentration of DWs, one can note the appearance of the Dirac-like gapless dispersion crossing the exchange energy gap. Under the higher concentration, the Dirac-like spectrum becomes gapped (i.e., with the "reduced" gap in the terms of Ref. [34] at the $\overline{\Gamma}$ point owing to the hybridization of the states bound to the neighboring DWs (see Fig. 4 and the corresponding comments). From that standpoint, the disagreement of the ARPES findings for the surface spectra of intrinsic AFM TI $MnBi_2Te_4$ can be attributed to the growth conditions and magnetic treatment of tested samples.

The disagreement between some spectroscopic probes indicating a relatively large exchange gap at the TI surface and the low-temperature range of the QAHE realization remains an important matter [68]. The quantized conductivity effects in real systems are affected by a complex network of topologically nontrivial and trivial conducting channels running along boundaries, separating regions of distinct topological phases [69]. Our results demonstrate the presence of the DW-induced states embodying the conducting channels at the magnetic surface of TI and describe their characteristics. In magnetotransport measurements, when the chemical potential is fixed within the energy gap, the conductivity is realized by means of both a carrier propagation along the edge channels of the sample and a percolation through 1D channels caused by the network of the magnetic DWs [41,70]. Therefore the measured conductivity can display remarkable deviation from the expected quantized value.

We have revealed a unique possibility to tune the group velocity and spin-polarization orientation of the DW-induced states by reorienting the easy-axis direction, which could be useful to design new devices with controlled propagation velocity and chirality for the robust excitations responsible for quantized dissipationless conductivity. We have predicted that, when the moments lie within the easy plane parallel to the TI surface plane, both the head-to-head and tail-to-tail planar textures generate the chiral zero-energy flatband state in the single-particle spectrum. Due to the flatness of the energy dispersion and respectively the large peak of DOS, this state could attract particular attention from the perspective of enhanced electron correlations. Thereby, the surface of the planar magnetic TI carrying the DWs could provide a unique platform for realizing phase transitions driven by instabilities of the unusual quasiparticles—the heavy chiral fermions with nontrivial topology. In particular, in such a system, it would be interesting to seek for the unconventional superconductivity with spin-triplet pairing [71] or triplet excitonic insulator [72].

To summarize, we have provided the physical picture to understand the nature and properties of the DW-induced states at the TI magnetic surface. Implying a rich domain texture of the surface, we have shown the existence of various topologically protected states stemming from the DWs. The relevance of our results is based on the fact that the properties of the DW-induced states are explained in terms of a general approach, and their description is material independent. It can be applied to the surfaces of intrinsic magnetic TIs and the interfaces in hetrostructures with induced magnetization under any direction of anisotropy axis. Further investigations of the interplay between domain texture and the surface fermion states in the magnetic TIs, especially via different experimental techniques, are strongly desired to open the way to realize novel quantum phenomena.

ACKNOWLEDGMENTS

E.V.C. acknowledges support from Saint Petersburg State University (Project ID No. 73028629). I.P.R. and V.N.M acknowledge support from Russian Science Foundation within Research Project No. 18-12-00169-p (the study of DW-induced topological surface states by tight-binding calculations and a model Hamiltonian approach, respectively).

---

[1] M. Z. Hasan and C. L. Kane, Rev. Mod. Phys. **82**, 3045 (2010).
[2] X.-L. Qi and S.-C. Zhang, Rev. Mod. Phys. **83**, 1057 (2011).
[3] Y. Ando, J. Phys. Soc. Jpn. **82**, 102001 (2013).
[4] H. Weng, R. Yu, X. Hu, X. Dai, and Z. Fang, Adv. Phys. **64**, 227 (2015).
[5] X. Kou, Y. Fan, M. Lang, P. Upadhyaya, and K. L. Wang, Solid State Commun. **215-216**, 34 (2015).
[6] C.-Z. Chang and M. Li, J. Phys.: Condens. Matter **28**, 123002 (2016).
[7] C.-X. Liu, S.-C. Zhang, and X.-L. Qi, Annu. Rev. Condens. Matter Phys. **7**, 301 (2016).
[8] Y. Tokura, K. Yasuda, and A. Tsukazaki, Nat. Rev. Phys. **1**, 126 (2019).
[9] Q. L. He, L. Pan, A. L. Stern, E. C. Burks, X. Che, G. Yin, J. Wang, B. Lian, Q. Zhou, E. S. Choi, K. Murata, X. Kou, Z. Chen, T. Nie, Q. Shao, Y. Fan, S.-C. Zhang, K. Liu, J. Xia, and K. L. Wang, Science **357**, 294 (2017).
[10] V. N. Men'shov, I. A. Shvets, and E. V. Chulkov, JETP Lett. **110**, 771 (2019).
[11] C.-Z. Chang, J. Zhang, X. Feng, J. Shen, Z. Zhang, M. Guo, K. Li, Y. Ou, P. Wei, L.-L. Wang *et al.*, Science **340**, 167 (2013).
[12] A. J. Bestwick, E. J. Fox, X. Kou, L. Pan, K. L. Wang, and D. Goldhaber-Gordon, Phys. Rev. Lett. **114**, 187201 (2015).
[13] M. Mogi, R. Yoshimi, A. Tsukazaki, K. Yasuda, Y. Kozuka, K. S. Takahashi, M. Kawasaki, and Y. Tokura, Appl. Phys. Lett. **107**, 182401 (2015).
[14] K. N. Okada, Y. Takahashi, M. Mogi, R. Yoshimi, A. Tsukazaki, K. S. Takahashi, N. Ogawa, M. Kawasaki, and Y. Tokura, Nat. Commun. **7**, 12245 (2016).
[15] M. Mogi, M. Kawamura, A. Tsukazaki, R. Yoshimi, K. S. Takahashi, M. Kawasaki, and Y. Tokura, Sci. Adv. **3**, eaao1669 (2017).
[16] M. Mogi, M. Kawamura, R. Yoshimi, A. Tsukazaki, Y. Kozuka, N. Shirakawa, K. S. Takahashi, M. Kawasaki, and Y. Tokura, Nat. Mater. **16**, 516 (2017).
[17] D. Xiao, J. Jiang, J.-H. Shin, W. Wang, F. Wang, Y.-F. Zhao, C. Liu, W. Wu, M. H. W. Chan, N. Samarth, and C.-Z. Chang, Phys. Rev. Lett. **120**, 056801 (2018).

[18] R. Watanabe, R. Yoshimi, M. Kawamura, M. Mogi, A. Tsukazaki, X. Z. Yu, K. Nakajima, K. S. Takahashi, M. Kawasaki, and Y. Tokura, Appl. Phys. Lett. **115**, 102403 (2019).

[19] M. M. Otrokov, T. V. Menshchikova, M. G. Vergniory, I. P. Rusinov, A. Y. Vyazovskaya, Y. M. Koroteev, G. Bihlmayer, A. Ernst, P. M. Echenique, A. Arnau, and E. V. Chulkov, 2D Mater. **4**, 025082 (2017).

[20] M. M. Otrokov, T. V. Menshchikova, I. P. Rusinov, M. G. Vergniory, V. M. Kuznetsov, and E. V. Chulkov, JETP Lett. **105**, 297 (2017).

[21] H. Deng, Z. Chen, A. Wołoś, M. Konczykowski, K. Sobczak, J. Sitnicka, I. V. Fedorchenko, J. Borysiuk, T. Heider, Ł. Pluciński, K. Park, A. B. Georgescu, J. Cano, and L. Krusin-Elbaum, Nat. Phys. **17**, 36 (2021).

[22] Y. Deng, Y. Yu, M. Z. Shi, Z. Guo, Z. Xu, J. Wang, X. H. Chen, and Y. Zhang, Science **367**, 895 (2020).

[23] M. M. Otrokov, I. P. Rusinov, M. Blanco-Rey, M. Hoffmann, A. Y. Vyazovskaya, S. V. Eremeev, A. Ernst, P. M. Echenique, A. Arnau, and E. V. Chulkov, Phys. Rev. Lett. **122**, 107202 (2019).

[24] C. Liu, Y. Wang, H. Li, Y. Wu, Y. Li, J. Li, K. He, Y. Xu, J. Zhang, and Y. Wang, Nat. Mater. **19**, 522 (2020).

[25] A. M. Shikin, A. A. Rybkina, D. A. Estyunin, D. M. Sostina, V. Y. Voroshnin, I. I. Klimovskikh, A. G. Rybkin, Y. A. Surnin, K. A. Kokh, O. E. Tereshchenko, L. Petaccia, G. Di Santo, P. N. Skirdkov, K. A. Zvezdin, A. K. Zvezdin, A. Kimura, E. V. Chulkov, and E. E. Krasovskii, Phys. Rev. B **97**, 245407 (2018).

[26] D. Rakhmilevich, F. Wang, W. Zhao, M. H. W. Chan, J. S. Moodera, C. Liu, and C.-Z. Chang, Phys. Rev. B **98**, 094404 (2018).

[27] T. Chen, W. Liu, F. Zheng, M. Gao, X. Pan, G. van der Laan, X. Wang, Q. Zhang, F. Song, B. Wang, B. Wang, Y. Xu, G. Wang, and R. Zhang, Adv. Mater. **27**, 4823 (2015).

[28] B. A. Assaf, F. Katmis, P. Wei, C.-Z. Chang, B. Satpati, J. S. Moodera, and D. Heiman, Phys. Rev. B **91**, 195310 (2015).

[29] S. H. Lee, Y. Zhu, Y. Wang, L. Miao, T. Pillsbury, H. Yi, S. Kempinger, J. Hu, C. A. Heikes, P. Quarterman, W. Ratcliff, J. A. Borchers, H. Zhang, X. Ke, D. Graf, N. Alem, C.-Z. Chang, N. Samarth, and Z. Mao, Phys. Rev. Research **1**, 012011(R) (2019).

[30] E. K. Petrov, V. M. Men'shov, I. P. Rusinov, M. Hoffmann, A. Ernst, M. M. Otrokov, V. K. Dugaev, T. V. Menshchikova, and E. V. Chulkov, Phys. Rev. B **103**, 235142 (2021).

[31] M. Getzlaff, *Fundamentals of Magnetism* (Springer-Verlag, Berlin, 2008).

[32] G. Bertotti, *Hysteresis in Magnetism* (Academic, San Diego, 1998).

[33] Y. Gong, J. Guo, J. Li, K. Zhu, M. Liao, X. Liu, Q. Zhang, L. Gu, L. Tang, X. Feng *et al.*, Chin. Phys. Lett. **36**, 076801 (2019).

[34] A. M. Shikin, D. A. Estyunin, I. I. Klimovskikh, S. O. Filnov, E. F. Schwier, S. Kumar, K. Miyamoto, T. Okuda, A. Kimura, K. Kuroda *et al.*, Sci. Rep. **10**, 13226 (2020).

[35] P. M. Sass, J. Kim, D. Vanderbilt, J. Yan, and W. Wu, Phys. Rev. Lett. **125**, 037201 (2020).

[36] F. Hou, Q. Yao, C.-S. Zhou, X.-M. Ma, M. Han, Y.-J. Hao, X. Wu, Y. Zhang, H. Sun, C. Liu, Y. Zhao, Q. Liu, and J. Lin, ACS Nano **14**, 11262 (2020).

[37] M. Liu, W. Wang, A. R. Richardella, A. Kandala, J. Li, A. Yazdani, N. Samarth, and N. P. Ong, Sci. Adv. **2**, e1600167 (2016).

[38] E. O. Lachman, A. F. Young, A. Richardella, J. Cuppens, H. R. Naren, Y. Anahory, A. Y. Meltzer, A. Kandala, S. Kempinger, Y. Myasoedov, M. E. Huber, N. Samarth, and E. Zeldov, Sci. Adv. **1**, e1500740 (2015).

[39] J. Wang, B. Lian, and S.-C. Zhang, Phys. Rev. B **89**, 085106 (2014).

[40] M. Allen, Y. Cui, E. Yue Ma, M. Mogi, M. Kawamura, I. C. Fulga, D. Goldhaber-Gordon, Y. Tokura, and Z.-X. Shen, Proc. Natl. Acad. Sci. U.S.A. **116**, 14511 (2019).

[41] X. Wu, D. Xiao, C.-Z. Chen, J. Sun, L. Zhang, M. H. W. Chan, N. Samarth, X. C. Xie, X. Lin, and C.-Z. Chang, Nat. Commun. **11**, 4532 (2020).

[42] H. Li, S.-Y. Gao, S.-F. Duan, Y.-F. Xu, K.-J. Zhu, S.-J. Tian, J.-C. Gao, W.-H. Fan, Z.-C. Rao, J.-R. Huang *et al.*, Phys. Rev. X **9**, 041039 (2019).

[43] Y.-J. Hao, P. Liu, Y. Feng, X.-M. Ma, E. F. Schwier, M. Arita, S. Kumar, C. Hu, R. Lu, M. Zeng *et al.*, Phys. Rev. X **9**, 041038 (2019).

[44] Y. J. Chen, L. X. Xu, J. H. Li, Y. W. Li, H. Y. Wang, C. F. Zhang, H. Li, Y. Wu, A. J. Liang, C. Chen, S. W. Jung, C. Cacho, Y. H. Mao, S. Liu, M. X. Wang, Y. F. Guo, Y. Xu, Z. K. Liu, L. X. Yang, and Y. L. Chen, Phys. Rev. X **9**, 041040 (2019).

[45] P. Swatek, Y. Wu, L.-L. Wang, K. Lee, B. Schrunk, J. Yan, and A. Kaminski, Phys. Rev. B **101**, 161109(R) (2020).

[46] M. M. Otrokov, I. I. Klimovskikh, H. Bentmann, D. Estyunin, A. Zeugner, Z. S. Aliev, S. Gaß, A. U. B. Wolter, A. V. Koroleva, A. M. Shikin *et al.*, Nature (London) **576**, 416 (2019).

[47] A. Zeugner, F. Nietschke, A. U. B. Wolter, S. Gaß, R. C. Vidal, T. R. F. Peixoto, D. Pohl, C. Damm, A. Lubk, R. Hentrich *et al.*, Chem. Mater. **31**, 2795 (2019).

[48] R. C. Vidal, H. Bentmann, T. R. F. Peixoto, A. Zeugner, S. Moser, C.-H. Min, S. Schatz, K. Kißner, M. Ünzelmann, C. I. Fornari *et al.*, Phys. Rev. B **100**, 121104(R) (2019).

[49] K. Yasuda, M. Mogi, R. Yoshimi, A. Tsukazaki, K. S. Takahashi, M. Kawasaki, F. Kagawa, and Y. Tokura, Science **358**, 1311 (2017).

[50] I. T. Rosen, E. J. Fox, X. Kou, L. Pan, K. L. Wang, and D. Goldhaber-Gordon, npj Quantum Mater. **2**, 69 (2017).

[51] X. Zhou, G. Liu, F. Cheng, Y. Li, and G. Zhou, Ann. Phys. **347**, 32 (2014).

[52] Y. Araki, A. Yoshida, and K. Nomura, Phys. Rev. B **94**, 115312 (2016).

[53] J. Zhang, Z. Liu, and J. Wang, Phys. Rev. B **100**, 165117 (2019).

[54] N. Varnava, J. H. Wilson, J. H. Pixley, and D. Vanderbilt, Nat. Commun. **12**, 3998 (2021).

[55] M. Sedlmayr, N. Sedlmayr, J. Barnaś, and V. K. Dugaev, Phys. Rev. B **101**, 155420 (2020).

[56] K. F. Garrity, S. Chowdhury, and F. M. Tavazza, Phys. Rev. Materials **5**, 024207 (2021).

[57] L. Fu, Phys. Rev. Lett. **103**, 266801 (2009).

[58] T. Rauch, M. Flieger, J. Henk, I. Mertig, and A. Ernst, Phys. Rev. Lett. **112**, 016802 (2014).

[59] B. Messias de Resende, F. C. de Lima, R. H. Miwa, E. Vernek, and G. J. Ferreira, Phys. Rev. B **96**, 161113(R) (2017).

[60] M. P. L. Sancho, J. M. L. Sancho, J. M. L. Sancho, and J. Rubio, J. Phys. F **15**, 851 (1985).

[61] J. Henk and W. Schattke, Comput. Phys. Commun. **77**, 69 (1993).

[62] K. Nomura and N. Nagaosa, Phys. Rev. Lett. **106**, 166802 (2011).

[63] P. Upadhyaya and Y. Tserkovnyak, Phys. Rev. B **94**, 020411(R) (2016).

[64] B. A. Volkov, B. G. Idlis, and M. S. Usmanov, Phys. Usp. **38**, 761 (1995).

[65] B. A. Volkov and O. A. Pankratov, JETP Lett. **43**, 130 (1986).

[66] A. Hubert and R. Schafer, *Magnetic Domains* (Springer-Verlag, Berlin, 1998).

[67] W. Nolting and A. Ramakanth, *Quantum Theory of Magnetism* (Springer-Verlag, Berlin, 2009).

[68] C. Kim, J. Denlinger, A. Kundu, G. Gu, and T. Valla, J. Appl. Phys. **129**, 083902 (2021).

[69] V. N. Men'shov, I. A. Shvets, and E. V. Chulkov, Phys. Rev. B **99**, 115301 (2019).

[70] M. Kawamura, M. Mogi, R. Yoshimi, A. Tsukazaki, Y. Kozuka, K. S. Takahashi, M. Kawasaki, and Y. Tokura, Phys. Rev. B **98**, 140404(R) (2018).

[71] A. P. Mackenzie and Y. Maeno, Rev. Mod. Phys. **75**, 657 (2003).

[72] G. Sethi, Y. Zhou, L. Zhu, L. Yang, and F. Liu, Phys. Rev. Lett. **126**, 196403 (2021).